

Process Optimization and Mechanism Study for Sulfur Recovery from High-Silica Phosphogypsum via Carbothermal Reduction Smelting

Yanyu Wang, Cuihong Hou,* Shuailiang Qi, Shouyu Gu, Hongquan Jing, Jianmeng Wu, Hongling Guan,* and Hui Zhang



Cite This: ACS Omega 2024, 9, 18526–18541

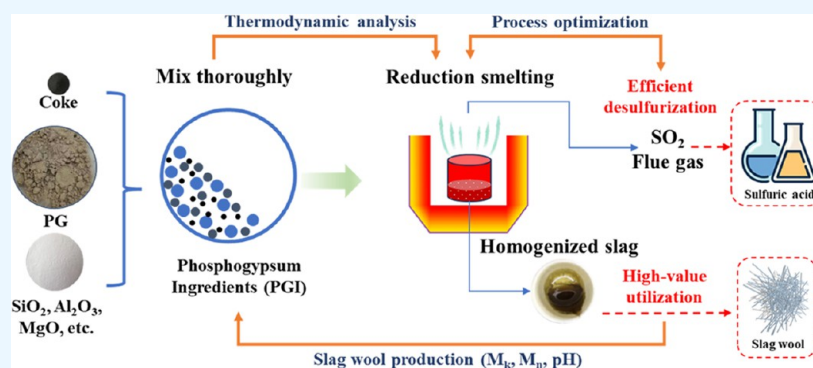


Read Online

ACCESS |

Metrics & More

Article Recommendations



ABSTRACT: Phosphogypsum produced from wet-processed phosphoric acid mainly consists of calcium sulfate dihydrate, which is an important sulfur resource. The traditional sulfuric acid and cement process based on phosphogypsum suffers from unstable cement quality owing to impurities such as phosphorus and fluorine and kiln ringing caused by the low-melting phase. This study investigated sulfur recovery and value-added utilization of liquid slag from high-silica phosphogypsum via carbothermal reduction smelting. A phosphogypsum ingredient (PGI) system was constructed by adding appropriate amounts of silica, alumina, magnesium oxides, and iron oxides to meet the production requirements of slag wool. Carbothermal reduction smelting experiments suggested that the temperature and C/S molar ratio significantly affected the desulfurization rate and phase structure of the slag. More than 97.44 wt % of sulfur could be recovered with a C/S molar ratio of 0.5–0.8 at 1300 °C or above in the molten state, and the molten slag was an amorphous magnesium–calcium–aluminosilicate. The PGI desulfurization mechanism is discussed based on the phase transformation and slag microstructure evolution.

1. INTRODUCTION

Phosphogypsum (PG) is a byproduct of wet-process phosphoric acid production, with 4.5–6 tons of phosphogypsum discharged per 1 ton of phosphate acid.^{1,2} Owing to the large-scale development of the phosphorus chemical industry, the annual discharge of phosphogypsum in China has reached 70 million tons.^{3,4} The storage of phosphogypsum results in land occupation and a severe threat to the surrounding ecological environment.⁵ Given this, harmless, reduced disposal, and cyclic utilization of phosphogypsum is urgently needed in the phosphorus chemical industry.⁶ Currently, phosphogypsum derived from phosphoric acid plant is extensively explored and utilized in construction materials,^{7–11} chemical industry,^{12–14} and agriculture.^{15,16}

SO₂ flue gas and cement clinker can be acquired from the process for sulfuric acid and cement based on phosphogypsum by adding clay, bauxite, and coke to the phosphogypsum,

followed by calcination in a rotary kiln. The process not only consumes plenty of phosphogypsum waste but also achieves the circulating utilization of sulfur and calcium resources,^{17–21} which retains practical significance and economic benefits considering the serious sulfur shortage in China.²² However, this process produces liquid phases at the burning temperature of the clinker, which wraps the phosphogypsum to decrease the decomposition rate and causes ring formation in the rotary kiln.²³ Simultaneously, the presence of impurities, such as phosphorus and fluorine, severely retards the setting time of

Received: February 3, 2024

Revised: March 24, 2024

Accepted: April 1, 2024

Published: April 9, 2024



the cement and reduces the early strength, causing unstable cement quality.^{24,25}

Currently, these problems are generally minimized by reducing the operating temperature or increasing the melting characteristics of the materials to significantly reduce the amount of liquid phase, thus avoiding crust blockage in the kiln. Simultaneously, some byproducts without strict restrictions on phosphorus and fluorine contents were adopted to solve the problem of unstable product quality. For example, the process of producing sulfuric acid and lime based on phosphogypsum was proposed, in which the phosphogypsum was calcined below 1200 °C directly without adding other raw materials. This reduced the content of Si, Al, Na, F, Cl, and other elements so that the lowest eutectic point of the raw materials was >1200 °C.²⁶ The process of preparing cementitious material with phosphogypsum-activated carbon and relatively small fly ash was developed in which the optimum operating temperature was set at 1200–1250 °C and phosphogypsum was partially decomposed to improve the easy burning properties of the material.²⁷ These operations alleviated the problem of kiln ringing owing to the formation of low-melting-point phases by lowering the operating temperature; however, this causes incomplete phosphogypsum decomposition. Additives were added to increase the melting characteristics of the material to avoid kiln ringing during the firing of the cement clinker. Kaolin and potassium feldspar increase the molten temperature during the reduction of phosphogypsum to avoid sintering.²⁸ However, eradicating the liquid phase completely is difficult owing to the material complexity at the cement clinker firing temperature during actual production.

The silicon dioxide content in calcium phosphate rock in China is ~15%, most of which enters the phosphogypsum during the wet process of phosphoric acid production. The high silica content leads to an unstable quality when phosphogypsum is used in gypsum building materials.² During the decomposition and recovery of sulfur resources and cement from phosphogypsum, a high silicon dioxide content affects the thermal decomposition process of PG and the properties of cement products.^{29,30} The high silicon dioxide content of phosphogypsum is a restricting factor for its cyclic utilization, and the removal of silica impurities from phosphogypsum is challenging because of the insolubility and coarse particle size of silica.³¹ SiO₂ is extracted and removed from high-silica phosphogypsum using a flotation method,^{32,33} which leads to increased costs and new waste. Yang et al. studied the direct application of chemical looping gasification (CLG) with a high-silicon PG oxygen carrier, in which SiO₂ participated in the production of syngas and inhibited the production of H₂S, which is desirable for clean production processes.³⁴ However, a relatively small dosage cannot solve the problem of large amounts of phosphogypsum.

The carbothermal reduction smelting process is used to extract valuable elements under melting conditions and exhibits the advantages of a high reduction efficiency and liquid slag discharge. The obtained molten slag can be modified to produce slag wool with a higher added value. Slag wool, a wool-like mineral fiber, primarily comprises 36–42 wt % SiO₂, 28–47 wt % CaO, 9–17 wt % Al₂O₃, 3–12 wt % MgO, and a minor amount of iron oxidation. It is produced from molten slag via centrifugal/blowing processes.^{35–39} The molten slag with an amorphous structure for producing slag wool should also simultaneously meet the requirements of

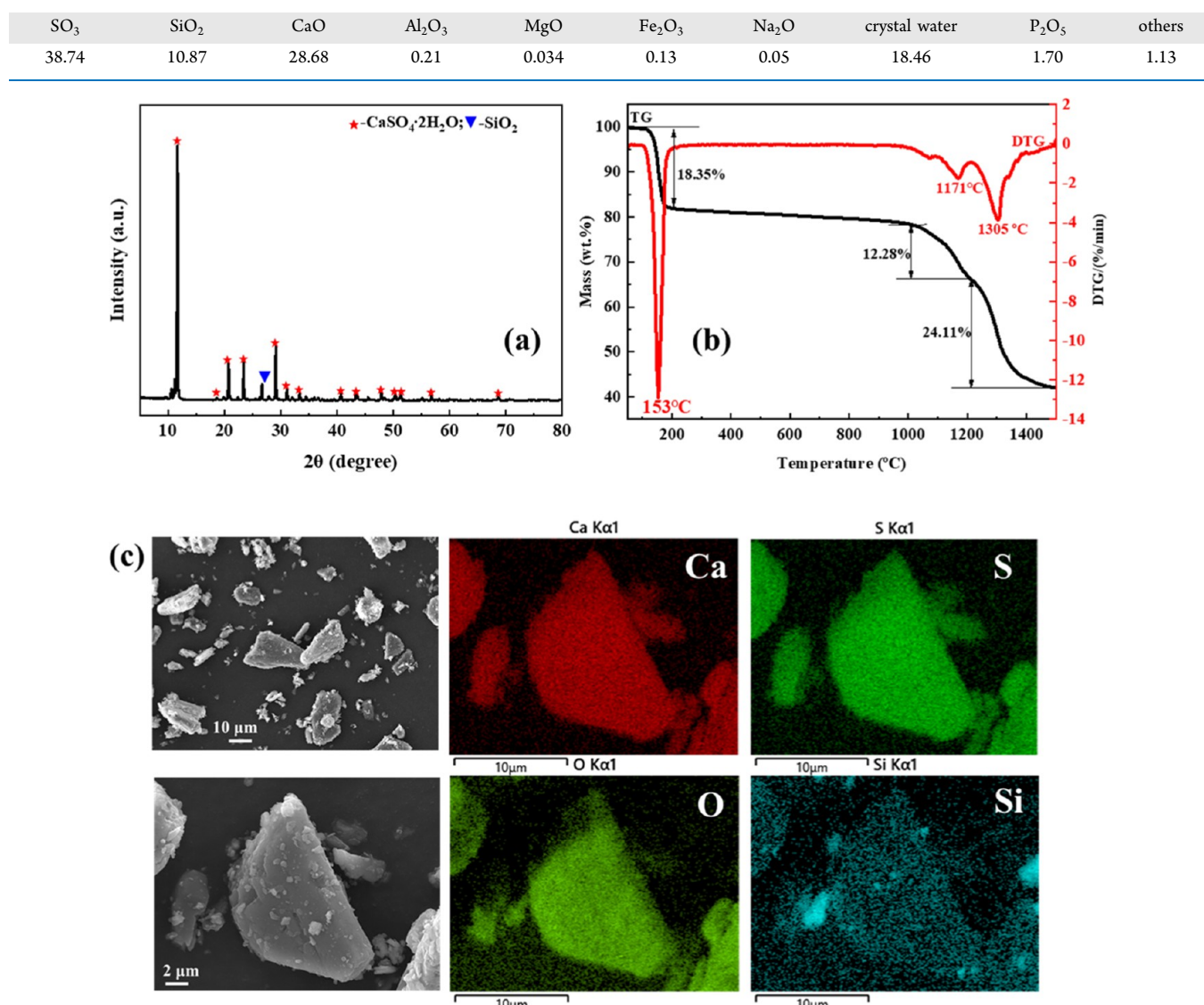
acidity coefficient (M_k), viscosity coefficient (M_η), and hydrogen ion index value (pH).^{40,41}

By increasing the operating temperature of the traditional process of phosphogypsum-based acid production, phosphogypsum can be decomposed under molten conditions, which can result in liquid slagging to solve the problem of kiln ringing. Simultaneously, the molten slag obtained could be used for the production of slag wool. Based on this, a coprocess of acid-making and slag wool production based on phosphogypsum via carbothermal reduction smelting was proposed in this study to achieve the circulating recovery of sulfur. High-silica phosphogypsum, mainly composed of calcium sulfate dihydrate and SiO₂, could meet the composition requirements of slag wool by adding some industrial solid wastes high in silica, alumina, and magnesium oxide, such as blast furnace slag and fly ash. In the resulting materials, sulfur could be recycled efficiently via carbothermal reduction smelting for sulfur acid production, and molten slag could be used for producing high-value-added slag wool. The carbothermal reduction decomposition of phosphogypsum is complex because of side reactions,⁴² and the influence of added ingredients on the melting characteristics and decomposition process of the system, which is crucial for process conditions and sulfur recycling, is one of the focuses of the study. The residual sulfides in the molten slag after reduction smelting can also affect the performance of prepared slag wool owing to hydration.⁴³ Therefore, the desulfurization rate and phase structure of slag are important indicators of the process. The recovery and development of industrial waste composites beneficial to the environment and economy are one direction for clean industrial production in the future.^{44,45}

In this study, a phosphogypsum ingredient (PGI) system with a low eutectic point was constructed by the thermodynamic analysis of the CaO–SiO₂–Al₂O₃–MgO quaternary slag phase diagram and determination of the melting characteristics. The obtained slag met the component requirements of slag wool production. Considering that the quantity of the reducing agent and reaction temperature significantly impact the types of reaction products and desulfurization rate during the carbothermal reduction of phosphogypsum,^{46,47} this study investigated the thermal decomposition process of phosphogypsum ingredients at different C/S molar ratios by thermogravimetric-differential scanning calorimetry (TG-DSC). Process optimization was conducted by exploring the effects of the reaction time, temperature, and C/S molar ratio on the desulfurization rate and phase structure of the slags by the reduction smelting experiments. The PGI desulfurization mechanism was discussed by investigating the phase transformation and microstructure evolution of the PGI by using X-ray diffraction (XRD), X-ray photoelectron spectroscopy (XPS), and scanning electron microscopy–energy dispersive spectroscopy (SEM-EDS) characterization. This study provides an innovative method for optimizing sulfur recovery and amorphous slag formation from phosphogypsum by carbothermal reduction smelting in which efficient sulfur recovery and high-value slag utilization based on high-Si phosphogypsum were realized.

2. MATERIALS AND METHODS

2.1. Materials. Phosphogypsum used in this study was obtained from a phosphorus chemical enterprise in Yunnan Province, China. After being dried at 45 °C, it was crushed and ground for chemical composition analysis. The crystalline

Table 1. Chemical Compositions of Phosphogypsum/wt %**Figure 1.** (a) XRD pattern, (b) TG-DTG curves, and (c) SEM-EDS of high-silica phosphogypsum.

water content was determined by measuring the mass loss of the material drying at 230 $^{\circ}\text{C}$ for 1 h. The phosphogypsum was of the dihydrate type, with total CaO and SO_3 contents of 28.68 and 38.74 wt %, respectively, as shown in Table 1. The main impurities included 10.87 wt % SiO_2 , 1.70 wt % P_2O_5 , 0.21 wt % Al_2O_3 , and 0.13 wt % Fe_2O_3 , which belongs to high-silica phosphogypsum. XRD characterization showed that the main minerals are $\text{CaSO}_4\cdot 2\text{H}_2\text{O}$, along with an amount of quartz, as shown in Figure 1a. The TG-DTG curves of high-silica phosphogypsum (Figure 1b) indicated that phosphogypsum began to decompose at ~ 1000 $^{\circ}\text{C}$, and the reaction rate accelerated with temperature, but the decomposition was not yet complete at 1500 $^{\circ}\text{C}$. The SEM-EDS spectrum of phosphogypsum is shown in Figure 1c, with a plate-like structure, and impurities and SiO_2 particles distributed on the surface.

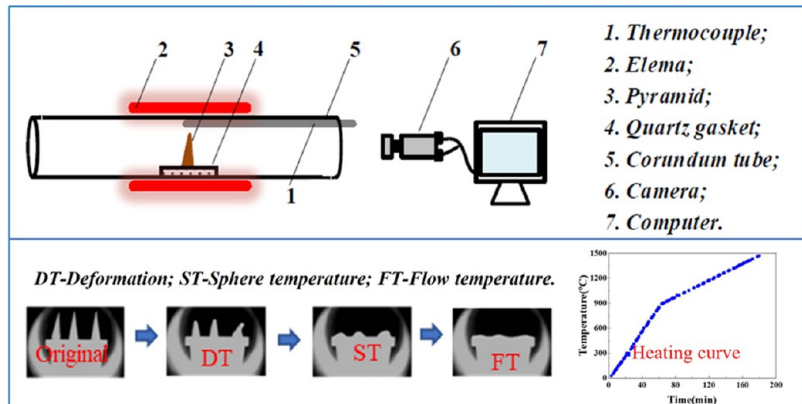
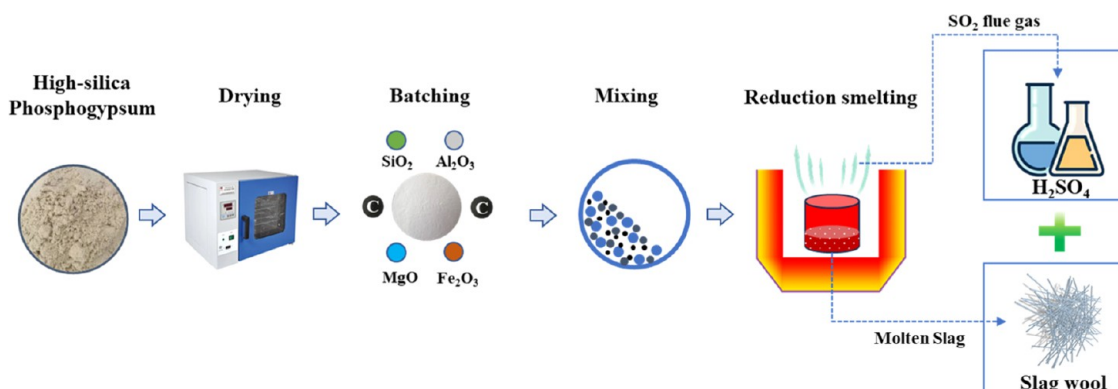
MgO powder and Al_2O_3 powder were purchased from Tianjin Comio Chemical Reagent Co., Ltd.; SiO_2 powder was purchased from Sinopharm Chemical Reagent Co., Ltd.; and Fe_2O_3 powder was purchased from Rhawn Reagent (Shanghai)

Co., Ltd. These reagents were chemically pure (>99.0 wt %), and they were added into phosphogypsum to build a system that met the production requirements of slag wool. Simultaneously, high-purity graphite powder with 99.95 wt % purity from Macklin Reagent Co., Ltd. was used for the carbon source in TG analysis, and industrial coke powders with fixed carbon of 79.20 wt % were used as reductants in high-temperature reduction experiments. N_2 (99.99% purity) was used as the sweep gas and shield gas in TG analysis, while N_2 (99.0% purity) was used for the reduction experiments.

2.2. Experimental Section. **2.2.1. Phosphogypsum Ingredient (PGI) System.** Herein, the PGI system was prepared in which analytically pure SiO_2 , Al_2O_3 , MgO , and Fe_2O_3 were added to phosphogypsum to meet the empirical parameters for the raw material requirements for slag wool production. The requirements are as follows: quaternary acidity coefficient (M_k) is 1.1–1.4, viscosity coefficient (M_η) is 1–3 Pa·s, and hydrogen ion index (pH) is 4–5, according to statistical data.⁴⁸ M_k is an important indicator for measuring the fiber-forming performance and physicochemical properties of slag wool, and M_η is

Table 2. PGI with Different Quaternary Acidities (M_k)

samples	M_k	PG/g	SiO_2/g	$\text{Al}_2\text{O}_3/\text{g}$	MgO/g	$\text{Fe}_2\text{O}_3/\text{g}$	pH	M_η
PGI-1.16	1.16	8.0	1.8	1.22	1.10	0.10	4.88	1.00
PGI-1.2	1.20	8.0	1.8	1.17	0.95	0.10	4.85	1.04
PGI-1.3	1.30	8.0	1.8	1.10	0.65	0.10	4.72	1.15
PGI-1.4	1.40	8.0	1.8	0.90	0.30	0.10	4.85	1.27

**Figure 2.** Schematic diagram of ash fusion temperature determination for materials.**Figure 3.** Experimental flowchart of this study.

used to characterize the fluidity of the slag, while pH is a more accurate indicator for measuring the chemical stability (atmospheric and water resistance) of slag fibers. Raw materials within an appropriate range of these three parameters can be used for producing qualified slag wool fibers. The calculation formulas are given in eqs 1–3.

$$M_k = \frac{\omega_{\text{SiO}_2} + \omega_{\text{Al}_2\text{O}_3}}{\omega_{\text{CaO}} + \omega_{\text{MgO}}} \quad (1)$$

$$M_\eta = \frac{M_{\text{SiO}_2} + 2M_{\text{Al}_2\text{O}_3}}{2M_{\text{Fe}_2\text{O}_3} + M_{\text{FeO}} + M_{\text{CaO}} + M_{\text{MgO}} + M_{\text{K}_2\text{O}} + M_{\text{Na}_2\text{O}}} \quad (2)$$

$$\text{pH} = -0.0602\omega_{\text{SiO}_2} - 0.120\omega_{\text{Al}_2\text{O}_3} + 0.232\omega_{\text{CaO}} + 0.120\omega_{\text{MgO}} + 0.144\omega_{\text{Fe}_2\text{O}_3} + 0.217\omega_{\text{Na}_2\text{O}} \quad (3)$$

where ω_{SiO_2} , $\omega_{\text{Al}_2\text{O}_3}$, ω_{CaO} , ω_{MgO} , $\omega_{\text{Fe}_2\text{O}_3}$, and $\omega_{\text{Na}_2\text{O}}$ are the corresponding oxide mass ratios of the slag, wt %, and M_{SiO_2} ,

$M_{\text{Al}_2\text{O}_3}$, $M_{\text{Fe}_2\text{O}_3}$, M_{FeO} , M_{CaO} , M_{MgO} , $M_{\text{K}_2\text{O}}$, and $M_{\text{Na}_2\text{O}}$ are the corresponding oxide molar ratios of the slag.

The SiO₂, CaO, Al₂O₃, and MgO contents should also be within the range of the slag wool components. Some solid wastes, such as fly ash and blast furnace slag, usually contain a small amount of iron oxides, which have a certain impact on the pH value and viscosity of the slag according to eq 2 and 3, respectively. A series of iron oxide reactions occurred during carbothermal reduction. Therefore, only a small modest amount of Fe₂O₃ was added to the ingredients system in this study.

Assuming that the CaSO₄·2H₂O in the phosphogypsum completely decomposes into CaO at high temperature, when 8.0 parts (in mass) of PG was used, 1.8 part SiO₂, 0.9 part Al₂O₃, 0.3 part MgO, and 0.1 part Fe₂O₃ were added to meet the raw material requirements of slag wool production with the slag system $M_k = 1.40$, $M_\eta = 1.27$ Pa·s, and pH = 4.85. Phosphogypsum ingredients (PGI) with different quaternary acidity coefficients were also calculated, in which the amounts of phosphogypsum, SiO₂, and Fe₂O₃ were fixed, while different M_k systems were obtained by varying the dosages of alumina and magnesium oxide (Table 2).

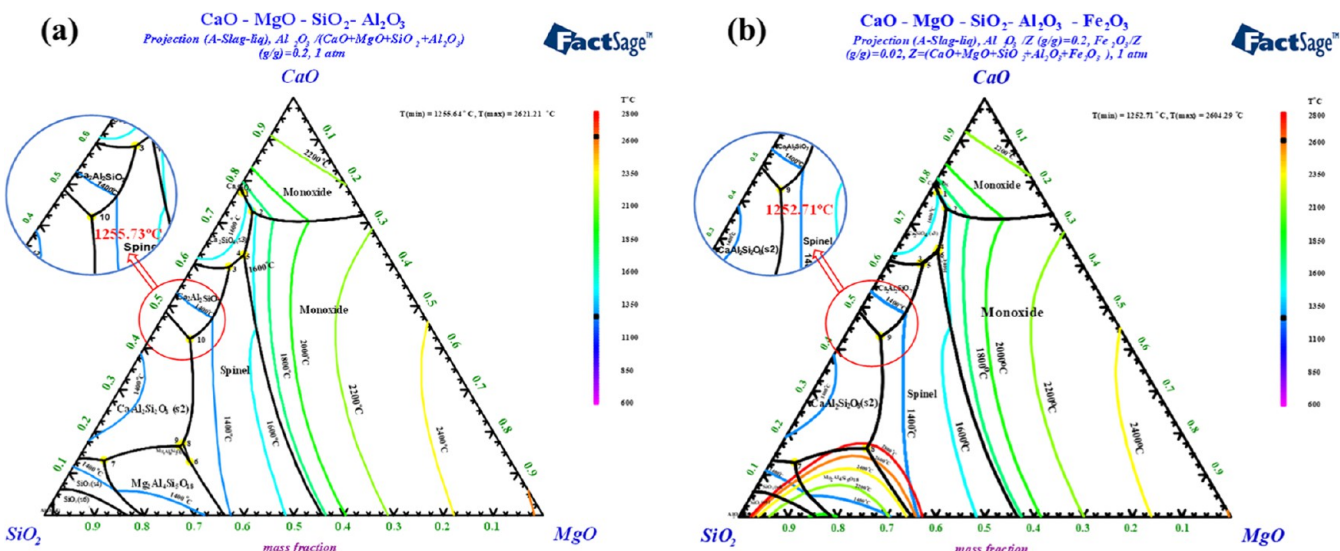


Figure 4. Phase diagrams calculated by FactSage software. (a) CaO–MgO–SiO₂–Al₂O₃ (Al₂O₃/(CaO + MgO + SiO₂ + Al₂O₃) (g/g) = 0.2, 1 atm); (b) CaO–MgO–SiO₂–Al₂O₃–Fe₂O₃ (Al₂O₃/Z (g/g) = 0.2, Fe₂O₃/Z (g/g) = 0.02, Z = (CaO + MgO + SiO₂ + Al₂O₃ + Fe₂O₃), 1 atm).

2.2.2. Determination of Ash Fusion Temperatures. The ash fusion temperatures of the PGI including deformation temperature (DT), sphere temperature (ST), and flow temperature (FT) were determined by a microcomputer ash melting point tester measuring range: 900–1500 °C; heating rate: 10 °C/min (room temperature ~900 °C), 5 °C/min (900–1500 °C) as shown in Figure 2. In this study, the raw materials (particle size <0.1 mm) were weighed, mixed, ground evenly in an agate mortar, and shaped into triangular cones with dimensions of 5 mm × 12 mm, and heated at the center of the furnace.

2.2.3. Reduction Smelting Experiments. The carbothermal reduction smelting test procedure included proportioning, mixing, melting, cooling, and grinding. The experimental flowchart of this study is shown in Figure 3. The reduction smelting experiments were conducted in a high-temperature atmosphere furnace, which was a sealed high-temperature electric furnace, with a maximum temperature of 1600 °C. In this study, N₂ gas was used as the flushing gas (protective atmosphere) with a flow rate of 4–5 dm³/min in the carbothermal reduction smelting tests, and the equipment diagram of the furnace was described in detail in our previous study.^{49,50} As shown in Table 2, the raw materials and coke powders with a designed C/S molar ratio were thoroughly mixed in certain ratios, and 22 g of the mixture was loaded into a corundum crucible. Before the carbothermal reduction smelting process, the furnace was heated to 1250 °C in advance, and N₂ gas was used as the flushing gas (protective atmosphere) with a flow rate of 4–5 dm³/min in the whole process. After melting at a designated temperature and time, the obtained samples were quickly cooled to room temperature in air, weighed, crushed, and ground into a fine powder for subsequent analysis and characterization.

The PG and PGI-1.4 with a C/S molar ratio of 0.5 were reduced at 800, 900, 1000, and 1100 °C for 20 min. The experimental conditions were the same as those used in the reduction smelting tests described above.

2.3. Characterization. **2.3.1. Desulfurization Rate.** The desulfurization rate of phosphogypsum ingredients (PGIs) is calculated using eq 4. The desulfurization rate refers to the sulfur distribution ratio of the flue gas. In this study, the

desulfurization rate was calculated by analyzing the total sulfur content of the slag. The total sulfur content of slag was determined by using chemical analysis according to the China National Standard GB/T 1549–2008 procedure. The samples were dissolved by heating with sodium hydroxide and extracted with hot water for chemical analysis using the barium sulfate precipitation gravimetric method.

$$\Phi = \left(1 - \frac{\omega_2 \times m_2}{\omega_1 \times m_1} \right) \times 100\% \quad (4)$$

where Φ is the desulfurization rate of PGI, wt %; ω_1 is the SO₃ content of PG, wt %; m_1 is the mass of PG in the PGI system, g; ω_2 is the total S content (calculated as SO₃) of slag, wt %; and m_2 is the mass of slag, g.

2.3.2. Decomposition Rate. The decomposition rate of PG and PGIs is calculated using eq 5. The decomposition rate refers to the decomposition ratio of calcium sulfate in the sample. The decomposition rate was calculated by analyzing the SO₃ content of the slag. The SO₃ content of slag was determined according to the China National Standard GB/T 5484–2012 procedure. The samples were extracted by heating with 1 + 1 HCl solution for chemical analysis using the barium sulfate precipitation gravimetric method.

$$\varphi = \left(1 - \frac{\omega_3 \times m_2}{\omega_1 \times m_1} \right) \times 100\% \quad (5)$$

where φ is the decomposition rate of PG or PGI, wt %; ω_1 is the SO₃ content of PG, wt %; m_1 is the mass of PG in the raw materials, g; ω_3 is the SO₃ content of slag, wt %; and m_2 is the mass of slag, g.

2.3.3. Instrument Analysis. The main phase identification of the PG and reduction slags was performed using XRD with a D/MAX-2200 X-ray diffractometer (Rigaku 94 Co.) with Cu K α radiation ($\lambda = 0.15406$ nm) at a scanning rate of 10°/min from 10 to 90° (2 θ). To study the microstructures of the slag, cooled samples were heat-mounted in resin and polished to a section with a mirror surface. The polished sections were studied using SEM (TESCAN MIRA LMS) equipped with electron dispersive spectroscopy (EDS) for spot, line, and map

scanning analyses to reveal the element distribution and migration. The acceleration voltages for morphology and energy spectrum mapping were 30 and 15 kV, respectively, and the detector was an SE2 secondary electron detector. Samples obtained were tested to determine the chemical state of S and Fe elements on the surface of the reduced samples by XPS (Thermo ESCALAB 250XI) under the following conditions: Al $\text{K}\alpha$, filament current, and voltage: 13.5 mA, 14.6 kV; passing energy: 20 eV; step size: 0.1 eV; perform 20 cycles of signal accumulation. All spectra were calibrated using the C 1s = 284.8 eV binding energy as the energy standard.

The PGIs with different C/S molar ratios were analyzed by using TG-DSC. Thermogravimetric studies were performed using a Netzsch STA449F5 thermal analyzer operated in a nitrogen atmosphere at a heating rate of 10 °C/min. The CaO–MgO–SiO₂–Al₂O₃ and CaO–MgO–SiO₂–Al₂O₃–Fe₂O₃ phase diagrams and gas production of the CaSO₄ ingredients system at different C/S molar ratios were calculated using thermodynamic calculations (FactSage 8.2). The “Phase Diagram” and “Equilib” modules were adopted, and the used databases were ‘FToxid’, ‘FactPS’, and ‘FTsalt.’ The pressure used for the FactSage calculations was 1 atm.

3. RESULTS AND DISCUSSION

3.1. Thermodynamic Analysis of the PGI System. In this study, SO₂ flue gas and slag were obtained by the carbothermal reduction smelting of PGIs, and the melting point determination was a prerequisite for the reduction smelting process. The proportions of Al₂O₃ and Fe₂O₃ were set according to PGI-1.4 in Table 2.

From the CaO–MgO–SiO₂–Al₂O₃ phase diagram, the formation of gehlenite (Ca₂Al₂SiO₇), anorthite (CaAl₂Si₂O₈), and spinel (MgAl₂O₄) induces the lowest melting point of the quaternary system of 1255 °C (point 10 in Figure 4a). The contents of CaO, MgO, SiO₂, and Al₂O₃ are 35.13, 6.72, 41.49, and 16.67 wt %, respectively, which correspond to a quaternary acidity of 1.39. Notably, from the CaO–MgO–SiO₂–Al₂O₃ phase diagram, the increase or decrease in SiO₂ corresponds to the same change in M_k when the Al₂O₃ content is constant, which can induce the generation of some high-melting-point phases, thus increasing the melting temperature of the slag system.²⁹ Comparison of Figure 4a,b confirms that the lowest melting point decreases from 1255 to 1252 °C (point 9 in Figure 4b) in the presence of 2.0 wt % Fe₂O₃. The presence of a small amount of Fe₂O₃ had a negligible effect on the lowest eutectic point.

The characteristic melting temperatures of PGI depend on the quaternary acidity (M_k), as shown in Figure 5. The temperatures of the system with M_k = 1.4 were lower than those with M_k = 1.16, 1.2, and 1.3, and the values of DT, ST, and FT of the system were 1230, 1246, and 1249 °C, respectively. These temperatures increased by 11–18 °C when M_k decreased to 1.3. The system with M_k = 1.16 had the highest characteristic melting temperature with DT, ST, and FT of 1262, 1274, and 1276 °C, respectively. The FT of PGI-1.4 is consistent with the lowest eutectic point in the CaO–MgO–SiO₂–Al₂O₃–Fe₂O₃ phase diagram. A follow-up study was conducted using a system with a quaternary acidity coefficient of 1.4.

3.2. Desulfurization Effect and Slag Phase Structure. The effects of residence time, temperature, and C/S molar ratio on desulfurization rate and slag phase structure were investigated by reduction tests of the PGI-1.4 in a high-

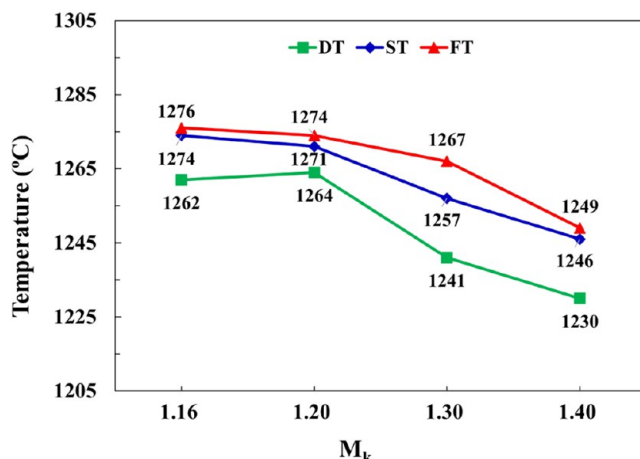


Figure 5. Ash fusion temperatures of PGIs with different quaternary acidity coefficients (M_k).

temperature atmosphere furnace. The preparation of slag wool by blowing or centrifugal processes was generally conducted at 1350–1550 °C under molten conditions. Based on the production process, the effect of reaction times on desulfurization rate and slag phase structure was first investigated at 1450 °C (200 °C above FT) in the study. The sulfur content of PGI-1.4 before processing was 27.92%. As shown in Figure 6a, the total sulfur content of the slags obtained at different times was all lower than 1.5 wt % and gradually decreased with time. The desulfurization rate of the system reached 97.29 wt % at 5 min and further raised to 98.85 wt % at 20 min, and changed a little when the time continued to 40 min. Therefore, a reaction time of 20 min was appropriate for the effectiveness and economy. The effects of the reaction temperature and C/S molar ratio on sulfur escape were further explored at a residence time of 20 min.

The total sulfur contents of the slags obtained at 1250, 1300, 1350, 1450, and 1550 °C for 20 min were investigated, and the desulfurization rates of the system were calculated as shown in Figure 6b. The results indicated that the material partially melted on the surface at 1250 °C and completely melted at 1300 °C. Consequently, the total sulfur content of the slag slid sharply from 6.12 to 1.24 wt %, with a corresponding rapid rise in the desulfurization rate from 86.51 to 97.44 wt %. The desulfurization rate of the system continued to increase but not significantly above 1300 °C. It can be concluded that the sulfur of the PGI-1.4 escaped rapidly and efficiently in the molten state, and the residual sulfur content of the slag was <1.5 wt %. In addition, the XRD pattern of slag formed at 1300 °C had no notable diffraction peaks and showed a good glassy phase, as shown in Figure 6d, with the basic conditions for further preparation of slag wool, which indicated that the process of jointly preparing sulfuric acid and slag wool based on phosphogypsum was theoretically feasible.

The desulfurization rate was discussed for C/S molar ratios of 0.3, 0.5, 0.8, 1.0, 1.2, and 2.0, respectively, as shown in Figure 6c. When the C/S molar ratio increased from 0.3 to 0.8, the desulfurization rate of the system increased slightly from 98.30 to 98.69 wt %. However, importantly, with a continuous increase in the C/S molar ratio, the desulfurization rate showed a noticeable downward trend. When the C/S molar ratio was 2.0, the total sulfur content in the slag rose to 4.99 wt %, and the corresponding desulfurization rate dropped to 90.22 wt %. This is mainly because when the C/S molar ratio is

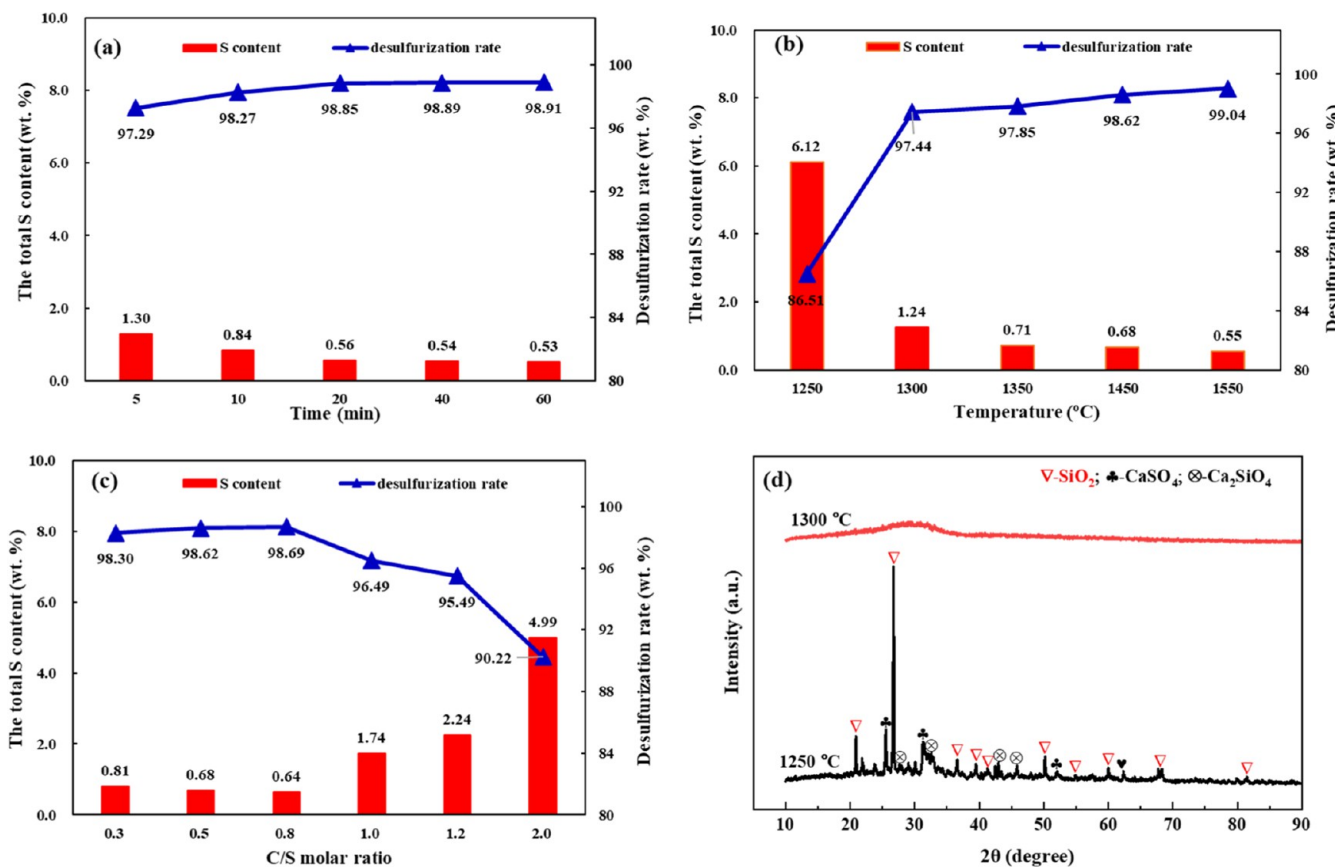


Figure 6. Effects of reaction conditions on the total sulfur content of slag and the desulfurization rate of PGI-1.4: (a) residence times ($1450\text{ }^{\circ}\text{C}$, $n_c/n_s = 0.5$); (b) temperatures (20 min, $n_c/n_s = 0.5$); (c) C/S molar ratios ($1450\text{ }^{\circ}\text{C}$, 20 min); (d) XRD patterns of slags obtained at 1250 and $1300\text{ }^{\circ}\text{C}$ for 20 min.

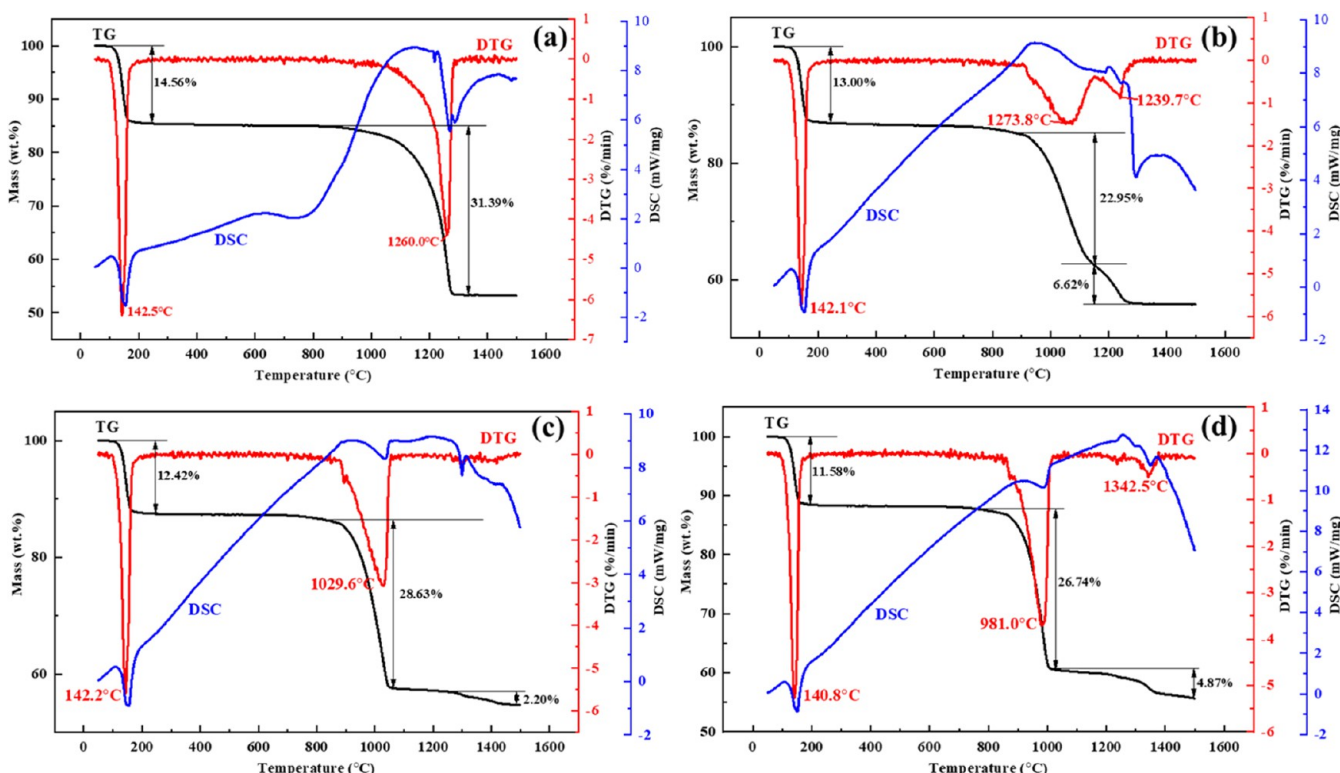


Figure 7. TG-DTG-DSC curves of PGI-1.4 with different C/S molar ratios: (a) $n_c/n_s = 0$; (b) $n_c/n_s = 0.5$; (c) $n_c/n_s = 1.0$; (d) $n_c/n_s = 2.0$.

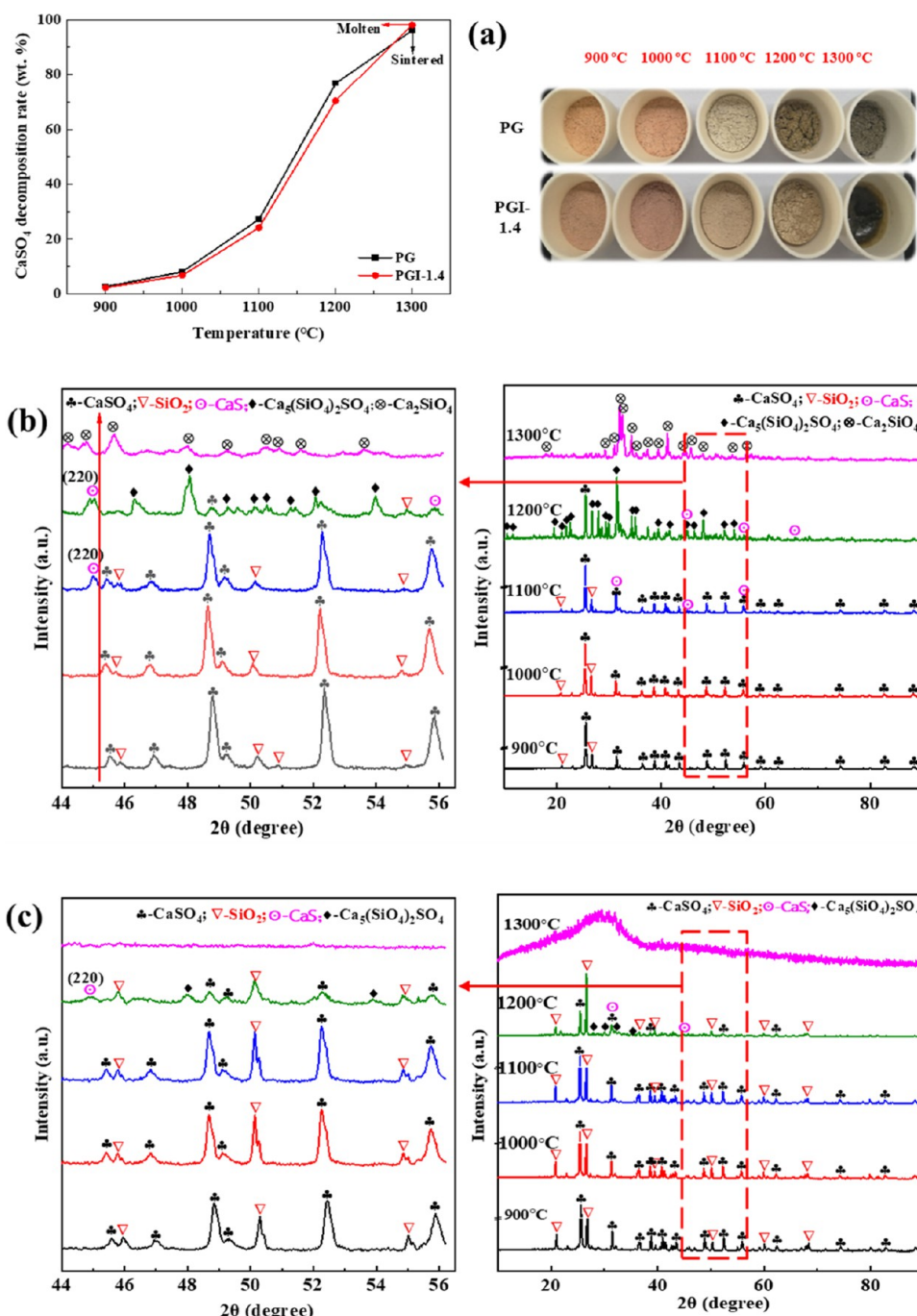


Figure 8. PG and PGI-1.4 with a C/S molar ratio of 0.5 reduced at $900\text{--}1300^{\circ}\text{C}$ for 20 min. (a) The decomposition rate of CaSO_4 ; (b) XRD patterns of PG; (c) XRD patterns of PGI-1.4.

low, less CaS is produced by C reduction of CaSO_4 , whereas the unreacted CaSO_4 oxidizes CaS into CaO and SO_2 . When more C is added, owing to the increase in CaS generated by the C reduction of CaSO_4 , the relative decrease in CaSO_4 leads to the sulfide residues in the slag, thereby reducing the desulfurization rate of the system.^{51,52}

In summary, it can be concluded that the amount of reducing agent and smelting temperature are the key factors affecting the desulfurization effect and slag phase structure in the new process of acid-making and slag wool production based on phosphogypsum. It was appropriate to add the reductant with a C/S molar ratio of 0.5–0.8, which was consistent with the previous research results.⁵³ The desulfur-

ization effect of phosphogypsum can be greatly improved in the molten state due to the enhanced mass and energy transfer. The XRD patterns of the slags obtained above 1300°C were all amorphous structures, which were the same as those at 1300°C in Figure 6d and were no longer listed.

3.3. Phase Transformation. The weight loss of PGIs during the heating process was studied by thermogravimetric analysis to further characterize the reaction process. The TG-DTG-DSC curves of PGI with $M_k = 1.4$ at C/S molar ratios of 0, 0.5, 1.0, and 2.0 were shown in Figure 7a–d. It can be seen that below 200°C , PG got rid of crystal waters and the weight loss decreased with the graphite addition, owing to the relative reduction of PG in the materials. The weight loss in the high-

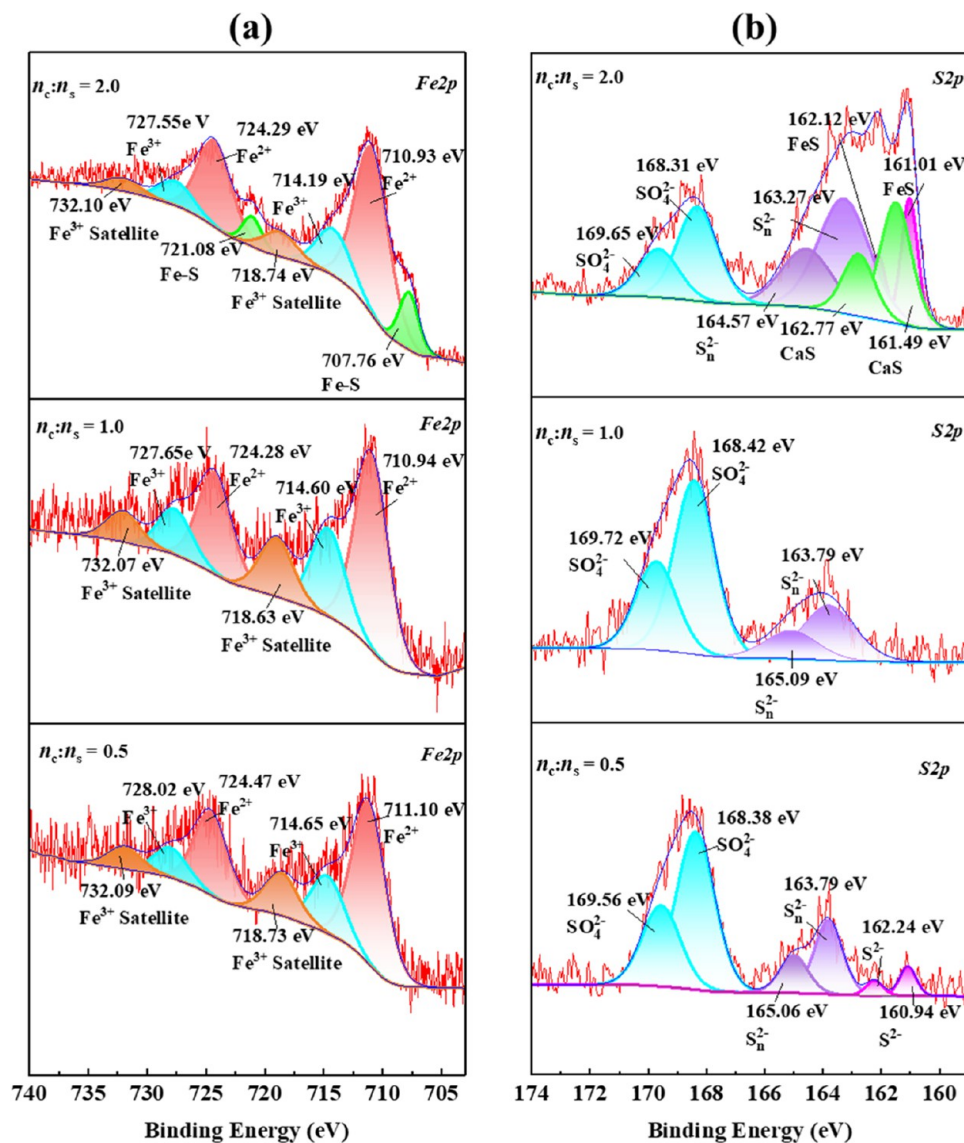
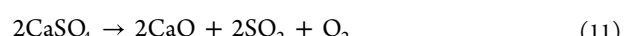
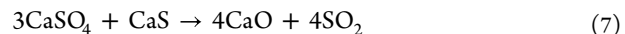
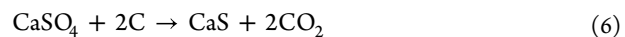


Figure 9. XPS analysis of PGI-1.4 with different C/S molar ratios reduced at 1450 °C for 20 min. (a) Slag preparation; (b) survey spectra; (c) high-resolution spectra of Fe 2p; and (d) high-resolution spectra of S 2p.

temperature zone (above 800 °C) was mainly attributed to the decomposition of PG. The addition of carbon significantly reduced the initial decomposition temperature and affected the decomposition process. Without the addition of carbon, the thermal decomposition of PG started only at 1000 °C, and the decomposition rate accelerated after 1100 °C and ended at 1273 °C with a weight loss of 31.39 wt % as shown in Figure 7a. When the C/S molar ratio was 0.5 (Figure 7b), the decomposition process was divided into two stages according to the two peaks of the DTG curve in the high-temperature stage. The first stage was mainly for C reduction of CaSO₄ to generate CaS and CO₂, and CaS and CaSO₄ further reacted to form CaO and SO₂ occurring simultaneously based on eqs 6 and 7,⁵⁴ and the peak temperature was 1073.8 °C. Meanwhile, CO could be generated during C reduction of CaSO₄, which would serve as the reducing gas to further reduce CaSO₄ based on eqs 9 and 10.²² The second peak was mainly attributed to the self-decomposition of CaSO₄ according to eq 11. Equation 8 represents the total reactions of eqs 6 and 7, in which the C/S molar ratio was 0.5, in terms of stoichiometry, during the

carbothermal reduction of CaSO₄. However, the carbothermal reduction of Fe₂O₃ and incomplete mixing of the materials can lead to excess CaSO₄ during the high-temperature process.



When the C/S molar ratio increased to 1.0 (Figure 7c) and 2.0 (Figure 7d), the corresponding DTG curve exhibited only one peak. This was mainly because the more graphite added, the more CaS generated by C reduced CaSO₄, and the reaction of CaS and CaSO₄ ended with the exhaustion of CaSO₄.

Several side reactions occur during the reduction roasting of the PGIs, such as the generation of intermediate products

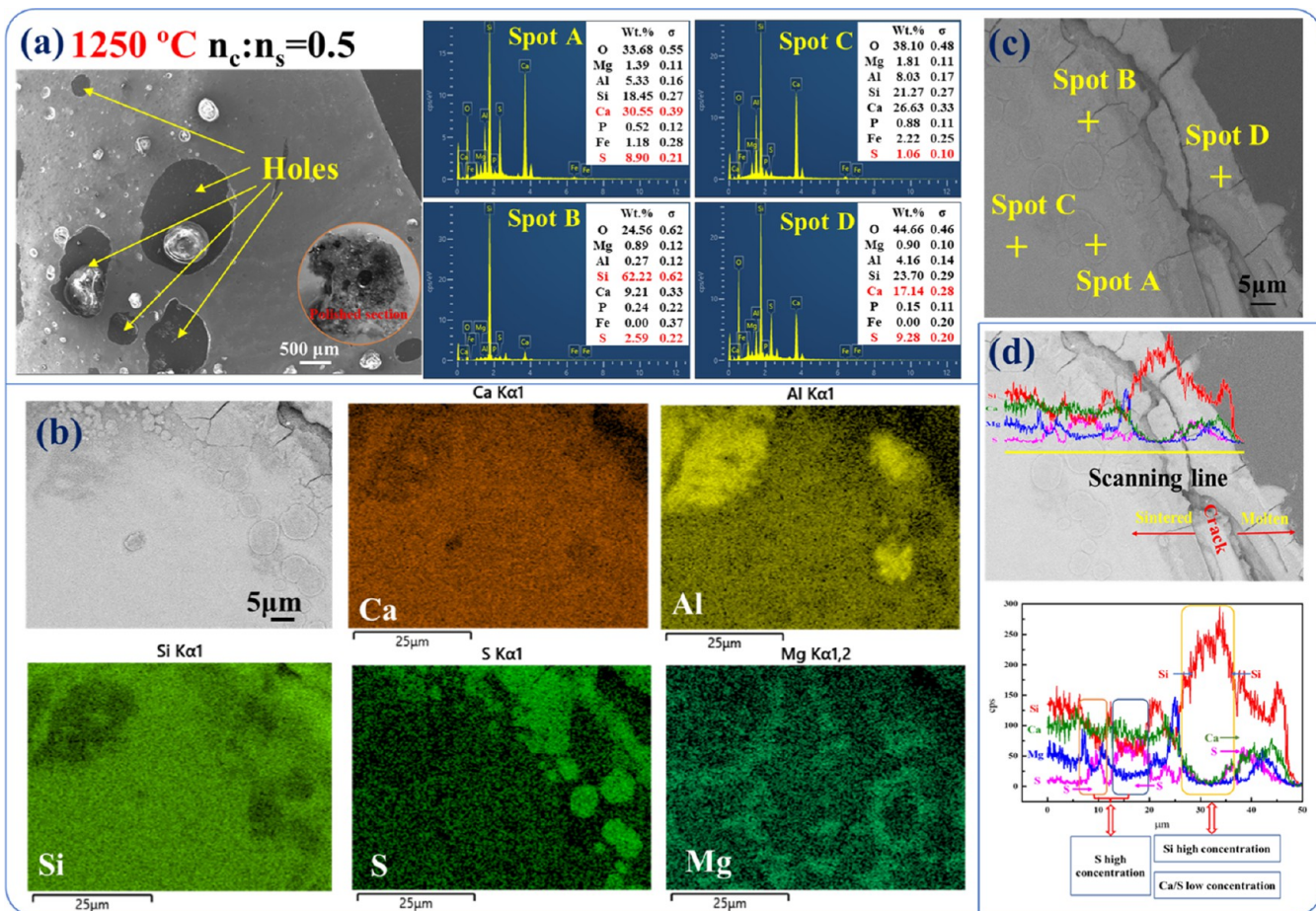


Figure 10. SEM-EDS analysis of the PGI-1.4 sample with a C/S molar ratio of 0.5 reduced at 1250 °C for 20 min. (a) SEM; (b) EDS element mapping; (c) SEM-EDS; (d) line scanning.

CaS⁴⁷ and the formation of new products owing to the addition of silica, alumina, and magnesium oxides that react with CaSO₄ or CaO, affecting the desulfurization effect of the system. Therefore, exploring the phase transformation during the reduction process is important. PG and PGI-1.4 were calcined at 900, 1000, 1100, 1200, and 1300 °C for 20 min, respectively, the decomposition rate of CaSO₄ and the XRD patterns are shown in Figure 8. Before 1100 °C, the decomposition rate of CaSO₄ in PGI-1.4 was not significantly different from that in PG, but increased between 1100 and 1275 °C. This was attributed to the formation of eutectic mixtures of calcium silicate, and calcium aluminate, which increased the liquid amount that encapsulated PG and hindered the reaction process.^{55,56} PGI-1.4 was completely molten at 1300 °C, and the decomposition rate increased significantly from 70.51 wt % at 1200 °C to 98.21 wt % at 1300 °C as shown in Figure 8a.

Figure 8b shows the XRD patterns of PG at a C/S molar ratio of 0.5 reduced at 900–1300 °C for 20 min. The characteristic diffraction peak intensity of CaSO₄ gradually decreased, indicating more decomposition. The left picture of Figure 8b shows that the characteristic diffraction peak of CaS (220) appeared at 1100 and 1200 °C, and then disappeared at 1300 °C. The study also proved that the decomposition of CaSO₄ proceeds in two steps as shown in eqs 6 and 7.⁵⁷ The characteristic diffraction peak of Ca₅(SiO₄)₂SO₄ (expressed as 2(Ca₂SiO₄)·CaSO₄) at 1200 °C showed that the calcium oxide deriving combined with silica and undecomposed CaSO₄. The

CaSO₄ and CaS phases at 1300 °C disappeared, and the final reduction product was mainly calcium silicate. Figure 8c shows the XRD patterns of PGI-1.4 reduced under a C/S molar ratio of 0.5 at 900, 1000, 1100, 1200, and 1300 °C, respectively, for 20 min. Although the overall phase transformations were consistent with those of PG, the characteristic peak of CaS was observed only at 1200 °C. At 1300 °C, the sample was completely melted, which was due to the successful construction of a low-melting-point eutectic system. This was confirmed by the amorphous diffraction peaks, which were the basis for preparing slag wool from molten slag.

The slags obtained from PGI-1.4 with C/S molar ratios of 0.5, 1.0, and 2.0 smelted at 1450 °C for 20 min were further investigated to clarify the reaction process. The valence states of Fe and S in the slag samples were investigated by using XPS. The reduced samples were cooled rapidly and crushed evenly to ensure uniformity. The high-resolution spectra of S and Fe were peak-fitted using Thermo Avantage software. The binding energies of the different element valence states are shown in Figure 9, which indicates the corresponding valence states of Fe and S in the outermost layer of the surface. In the high-resolution spectra of Fe 2p, as shown in Figure 9a, the peak at 707.76 eV was assigned to the binding energy of Fe²⁺ species bonded to sulfide,⁵⁸ and the peak at 710.92 eV was owing to the presence of FeSO₄,⁵⁹ when the C/S molar ratio was 2.0. The peak at 714.19 eV indicated the presence of Fe³⁺.⁶⁰ As shown in Figure 9b, the binding energies of S 2p_{2/3} peaks at 161.0–161.1 eV agree with what was generally found for the

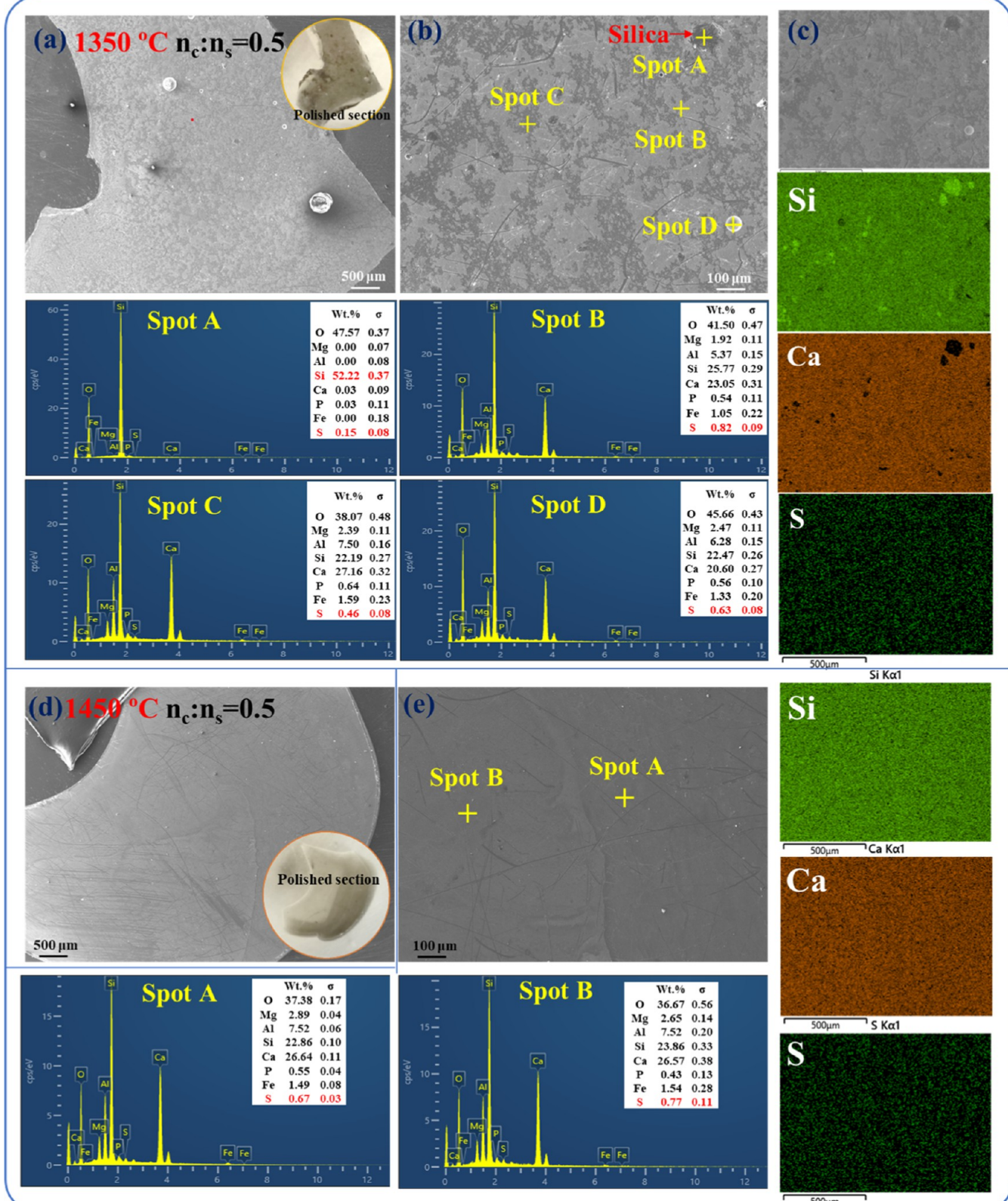


Figure 11. SEM-EDS analysis of PGI-1.4 samples with a C/S molar ratio of 0.5 reduced at 1350 and 1450 °C for 20 min. (a–c) SEM-EDS spectra at 1350 °C; (d, e) SEM-EDS spectra at 1450 °C.

monosulfide (S^{2-}) species of FeS ⁵⁸ and that at 161.49 eV was contributed by CaS .⁶¹ The peak at 163.27 eV was related to the formation of polysulfide (S_n^{2-} , $n > 2$).^{62,63} The peak at 168.31 eV corresponded to sulfate compounds, which could be

CaSO_4 or FeSO_4 .^{64–66} Comparing the intensities of the peaks, it was concluded that the amount of sulfide was lower than that of the sulfate when the C/S molar ratios were 0.5 and 1.0;

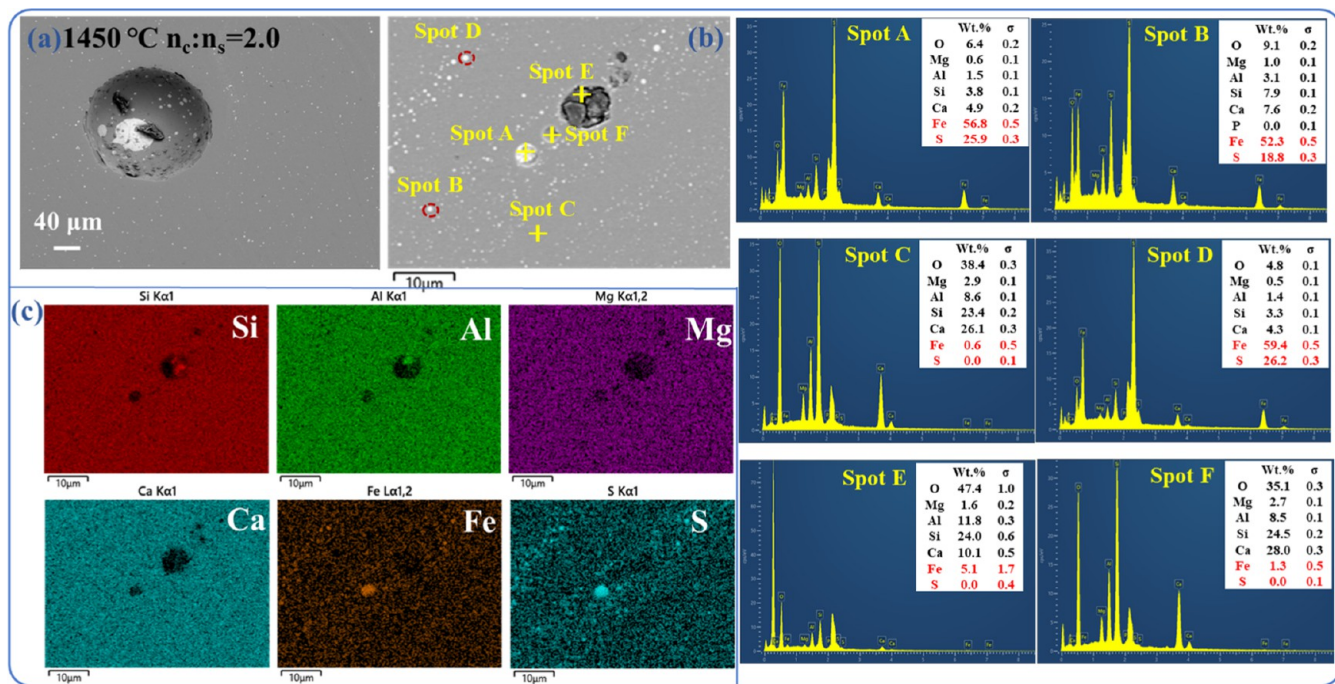


Figure 12. SEM-EDS analysis of the PGI-1.4 with a C/S molar ratio of 2.0 reduced at 1450 °C for 20 min: (a) SEM; (b) SEM-EDS; (c) EDS element mapping.

however, the content of sulfides was higher than that of the sulfates when the C/S molar ratio was 2.0.

3.4. Microstructure Evolution. The slag from PGI-1.4 at 1250 °C for 20 min was subjected to SEM-EDS to obtain the microstructure and chemical composition distribution of the microregions. The corresponding results for the longitudinal section of slag are shown in Figure 10.

As shown in Figure 10, when PGI-1.4 was reduced with a C/S molar ratio of 0.5 at 1250 °C for 20 min, the surface layer of the sample melted, and the interior appeared sintered, in which the generated gas diffused from the inside to the surface, forming a porous structure.⁶⁷ It can be seen from the line scanning that a crack emerged at the melting and sintering interface and aggregation of silicon at the molten interface. The high concentrations of S were attributed to the molten phase enveloping the surface of phosphogypsum, which hindered its further decomposition. Figure 10b,c showed the elemental distribution in the resultants and spot scanning. The Si, Al, and Mg elements in the slag were locally concentrated, particularly the sulfur element clustered at the interface. The S mass fractions of spots A and D were high at 8.90 and 9.28 wt %, respectively, while the corresponding mass fractions of Ca were 30.55 and 17.14 wt %. This also confirmed the obstruction of phosphogypsum decomposition and the aggregation of Si at the melting interface resulted in a relatively low Ca content. The S content of spot C was only 1.06 wt % because most CaSO₄ has decomposed at 1250 °C. These all indicated that the presence of liquid phases due to the addition of ingredients in phosphogypsum became a limiting factor for the desulfurization rate of the PGIs.

Figure 11 showed the distribution of the elements in the slag of PGI-1.4 with a C/S molar ratio of 0.5 at 1350 and 1450 °C for 20 min. As shown in Figure 11b, spot scanning revealed that the mass fraction of sulfur in the slag was less <1.0 wt %, which was the same as the result of the chemical analysis in Figure 6b. The increase in temperature decreased slag

viscosity, and enhanced fluidity is conducive to the decomposition of phosphogypsum and gas escape. Although the material melted, the microstructure showed a few holes and a small amount of unfused SiO₂ particles dispersed in the slag with an uneven distribution of elements. This proves that the formation of eutectic mixtures by adding SiO₂, Al₂O₃, and MgO reduces the melting point of the PGI system.⁵⁵ The map and spot scanning shown in Figure 11d,e demonstrated that Ca, Si, Al, and S were distributed uniformly in the slag obtained by the reduction smelting of PGI-1.4 at 1450 °C for 20 min. Homogeneous slag is a prerequisite for good fiber-forming performance.

The SEM-EDS analysis of PGI-1.4 at a C/S molar ratio of 2.0 reduced at 1450 °C for 20 min is shown in Figure 12. The SEM image showed that there were many lighter-colored particles embedded in the slag. According to the mapping and point scanning at Spot A, B, and D, it could be concluded that these particles should be the presence of FeS in the slag. This was mainly because iron oxide could be easily reduced to Fe²⁺ during the high-temperature process. When the C/S molar ratio was 2.0, the residual sulfides in the slag combined with Fe²⁺ to form FeS and a certain amount of polysulfides.⁶⁸ The high Fe content and the absence of S at Spot E indicated that iron also existed in other phase forms. The high contents of Si and Al in Spot E and the surrounding area could be attributed to unmelted SiO₂ and Al₂O₃ particles. It could be seen that when the C/S molar ratio was 2.0, the presence of more sulfides in the slag resulted in a lower desulfurization rate and poorer homogeneity of the slag, which was consistent with the results of chemical analysis and XPS characterization.

3.5. Discussion on the PGI Desulfurization Mechanism. Based on the aforementioned results, the PGI desulfurization mechanism and the formation of amorphous-structured slag are proposed and plotted in Figure 13. To recycle the maximum possible amount of sulfur from the waste PG and obtain the homogeneous slag suitable for producing

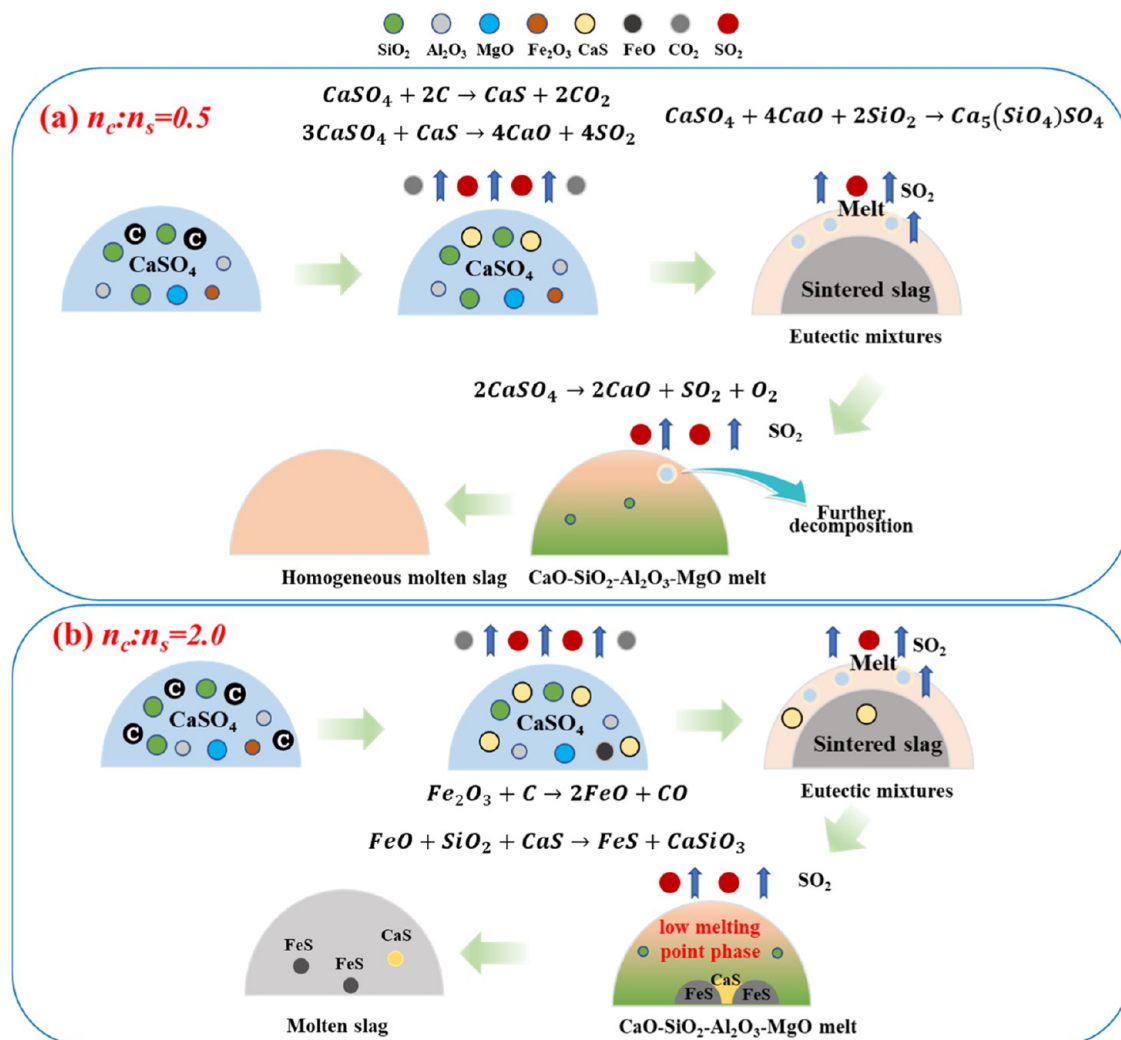
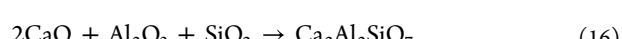
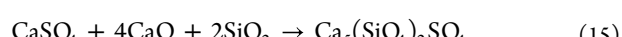
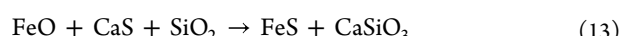


Figure 13. Schematic diagram of carbothermal reduction of PGI-1.4 with different C/S molar ratios. (a) $n_c/n_s = 0.5$; (b) $n_c/n_s = 2.0$. (Note: The reactions listed in (a) also occurred in (b)).

slag wool, the C/S molar ratio of 0.5–0.8 was extremely important, and the carbothermal smelting reduction temperature of 200 °C above FT was required. PGI was partially reduced to CaS according to eq 6. Then, CaS underwent a redox reaction with the undecomposed CaSO_4 to form CaO and SO_2 based on eq 7. When the C/S molar ratio was 1.0 or above, the generation of more CaS and relatively fewer CaSO_4 resulted in the sulfide residues in the slag, thereby reducing the desulfurization rate of the system. The divalent iron obtained by C reduction of iron trioxide (eq 12) is highly susceptible to binding with S^{2-} to form disulfide based on eq 13. Sulfides in slag are prone to hydration, which reduces their performance. Figure 13 shows the ideal state for the reaction. The experimental results indicated that both sulfides and sulfates existed in the slag, and the content and form of sulfur varied with the C/S molar ratio, as confirmed by XPS analysis. The actual reaction cannot be performed entirely in an ideal state because of uneven material mixing, however, this does not affect the reaction mechanism.

In the decomposition process of PG, the impurities SiO_2 and generated CaO react to generate Ca_2SiO_4 , which encapsulates CaSO_4 and hinders the reaction process based on eqs 14 and 15. This was also confirmed by the XRD pattern of PGI reduced at 1200 °C (Figure 8b) and the slag SEM-EDS at

1250 °C (Figure 10). Nevertheless, other materials such as SiO_2 , Al_2O_3 , and MgO combine with the generated CaO to form eutectic mixtures such as gehlenite ($\text{Ca}_2\text{Al}_2\text{SiO}_7$), anorthite ($\text{CaAl}_2\text{Si}_2\text{O}_8$), and spinel (MgAl_2O_4), based on eqs 16, 17, and 18, as illustrated in the $\text{CaO}-\text{MgO}-\text{SiO}_2-\text{Al}_2\text{O}_3$ phase diagram. As illustrated in Figure 10b, as the product amount increased, the mixture grew slowly to form a reaction surface that wrapped around the unreacted CaSO_4 . The materials quickly melted at 1300 °C, forming aluminosilicate glass. The molecular movement and mobility intensified in the melt further promoted the decomposition of CaSO_4 and considerably accelerated the outward diffusion rate of gas.



The smelting conditions of PGIs are also important for slag formation. The Si, Al, and other materials dispensed together with PG formed a eutectic system that promoted the efficient decomposition of CaSO_4 and sulfur escape under molten conditions, while the homogeneous molten phase discharged in liquid slag could be further used for the preparation of high-value-added slag wool.

4. CONCLUSIONS

This study investigated the decomposition process of phosphogypsum and slag microstructure during carbothermal reduction smelting via a PGI system construction and process optimization. The conclusions of the study are as follows:

- (1) The thermodynamic analysis indicated that a low eutectic system of melting point 1249 °C was constructed by collaborative utilization of silica, alumina, magnesium oxides, iron oxides, and phosphogypsum. The temperature and carbon-reductant addition played the dominant role in the PGI reduction process, and the optimum condition for sulfur escape and homogeneous slag was 1450 °C (200 °C above FT) for 20 min with a C/S molar ratio of 0.5–0.8. The desulfurization rate of PGI-1.4 was 98.62 wt %, and the slag was an amorphous structure with a uniform phase distribution.
- (2) Phase transformation and slag microstructure evolution are discussed to analyze the PGI desulfurization mechanism. PG is partially reduced to CaS, which further forms CaO and SO_2 . The addition of silica, alumina, and magnesium oxides combined with the generated CaO to form eutectic mixtures made the materials melt at 1300 °C, which promoted further self-decomposition of phosphogypsum and accelerated the SO_2 gas diffusion. The generation of more CaS and relatively less CaSO_4 formed sulfide residues in the slag, thereby reducing the desulfurization rate of the PGI system and the homogeneity of the slag.
- (3) This study provides a new method for efficiently recovering sulfur and high-value-utilizing slag from hazardous PG via carbothermal reduction smelting, as well as guides for industrialization trials. Simultaneously, it provides a new approach for collaborative utilization and resource recovery of industrial waste phosphogypsum and other solid wastes high in silicon, aluminum, and magnesium.

AUTHOR INFORMATION

Corresponding Authors

Cuihong Hou – School of Chemical Engineering, Zhengzhou University, Zhengzhou 450001 Henan, P. R. China;
Email: hch92@zzu.edu.cn

Hongling Guan – School of Chemical Engineering, Zhengzhou University, Zhengzhou 450001 Henan, P. R. China;
Email: guanhongling@zzu.edu.cn

Authors

Yanyu Wang – School of Chemical Engineering, Zhengzhou University, Zhengzhou 450001 Henan, P. R. China;
orcid.org/0009-0008-1189-8406

Shuailiang Qi – School of Chemical Engineering, Zhengzhou University, Zhengzhou 450001 Henan, P. R. China

Shouyu Gu – School of Chemical Engineering, Zhengzhou University, Zhengzhou 450001 Henan, P. R. China

Hongquan Jing – School of Chemical Engineering, Zhengzhou University, Zhengzhou 450001 Henan, P. R. China
Jianmeng Wu – School of Chemical Engineering, Zhengzhou University, Zhengzhou 450001 Henan, P. R. China;
orcid.org/0000-0002-9992-3897

Hui Zhang – Yunnan Yuntianhua Environmental Protection Technology Co., Ltd., Kunming 650000 Yunnan, P. R. China

Complete contact information is available at:

<https://pubs.acs.org/10.1021/acsomega.4c01100>

Author Contributions

Y.W.: Conceptualization, methodology, investigation, visualization, writing—original draft. C.H.: Visualization, writing—review and editing, funding acquisition. S.Q.: Methodology, investigation, visualization. S.G.: Conceptualization, project administration. H.J.: Conceptualization, visualization, writing—review and editing. J.W.: Visualization, writing—review and editing. H.G.: Visualization, investigation, writing—review and editing. H.Z.: Conceptualization, methodology, investigation.

Notes

The authors declare no competing financial interest.

ACKNOWLEDGMENTS

The authors express their heartfelt thanks to the Open Foundation of National Engineering and Technology Research Center for Development & Utilization of Phosphate Resources (NECP2022-02), the National Key Research and Development Program of China (nos. 2018YFC1900204 and 2018YFC1900200), the National Nature Science Foundation of China (21808212), China Postdoctoral Science Foundation (2019M652578), the Postdoctoral Sponsorship in Henan Province (1902015), and Yunnan Yuntianhua Environmental Protection Technology Co. for the financial support.

REFERENCES

- (1) Nedelciu, C. E.; Ragnarsdottir, K. V.; Schlyter, P.; Stjernquist, I. Global phosphorus supply chain dynamics: Assessing regional impact to 2050. *Global Food Secur.* **2020**, *26*, No. 100426.
- (2) Rashad, A. M. Phosphogypsum as a construction material. *J. Cleaner Prod.* **2017**, *166*, 732–743.
- (3) Qi, J.; Zhu, H.; Zhou, P.; Wang, X.; Wang, Z.; Yang, S.; et al. Application of phosphogypsum in soilization: a review. *Int. J. Environ. Sci. Technol.* **2023**, *20*, 10449–10464.
- (4) Ding, W.; Chen, Q.; Sun, H.; Peng, T. Modified mineral carbonation of phosphogypsum for CO_2 sequestration. *J. CO₂ Util.* **2019**, *34*, 507–515.
- (5) Agyei, N. M.; Strydom, C. A.; Potgieter, J. H. The removal of phosphate ions from aqueous solution by fly ash, slag, ordinary Portland cement and related blends. *Cem. Concr. Res.* **2002**, *32* (12), 1889–1897.
- (6) Ennaciri, Y.; Bettach, M. Procedure to convert phosphogypsum waste into valuable products. *Mater. Manuf. Process.* **2018**, *33* (16), 1727–1733.
- (7) Xiang, J. C.; Qiu, J. P.; Zheng, P. K.; Sun, X. G.; Zhao, Y. L.; Gu, X. W. Usage of biowashing to remove impurities and heavy metals in raw phosphogypsum and calcined phosphogypsum for cement paste preparation. *Chem. Eng. J.* **2023**, *451*, No. 138594.
- (8) Calderón-Morales, B. R.; García-Martínez, A.; Pineda, P.; García-Tenorio, R. Valorization of phosphogypsum in cement-based materials: Limits and potential in eco-efficient construction. *J. Build. Eng.* **2021**, *44*, No. 102506.
- (9) Fornés, I. V.; Vaičiukynienė, D.; Nizevičienė, D.; Doroševas, V.; Michalik, B. A comparative assessment of the suitability of

- phosphogypsum from different origins to be utilised as the binding material of construction products. *J. Build. Eng.* **2021**, *44*, No. 102995.
- (10) Murali, G.; Azab, M. Recent research in utilization of phosphogypsum as building materials: Review. *J. Mater. Res. Technol.* **2023**, *25*, 960–987.
- (11) Deng, F.; Ye, J.; Liu, Y. L.; Zhang, T. X.; Liao, Y. S.; Tang, S. W. Influence of cement on properties of calcined phosphogypsum based composite cementitious materials. *J. Mater. Res. Technol.* **2023**, *24*, 3145–3156.
- (12) Chen, Q. J.; Ding, W. J.; Sun, H. J.; Peng, T. J.; Ma, G. H. Indirect mineral carbonation of phosphogypsum for CO₂ sequestration. *Energy* **2020**, *206*, No. 118148.
- (13) Monat, L.; Chaudhury, S.; Nir, O. Enhancing the sustainability of phosphogypsum recycling by integrating electrodialysis with bipolar membranes. *ACS Sustainable Chem. Eng.* **2020**, *8* (6), 2490–2497.
- (14) Lambert, A.; Anawati, J.; Walawalkar, M.; Tam, J.; Azimi, G. Innovative application of microwave treatment for recovering of rare earth elements from phosphogypsum. *ACS Sustainable Chem. Eng.* **2018**, *6* (12), 16471–16481.
- (15) Costa, R. F.; Firmano, R. F.; Bossolani, J. W.; Alleoni, L. R. F. Soil chemical properties, enzyme activity and soybean and corn yields in a tropical soil under no-till amended with lime and phosphogypsum. *Int. J. Plant Prod.* **2023**, *17*, 235–250.
- (16) Samet, M.; Karray, F.; Mhiri, N.; Kamoun, L.; Sayadi, S.; Gargouri-Bouzid, R. Effect of phosphogypsum addition in the composting process on the physico-chemical properties and the microbial diversity of the resulting compost tea. *Environ. Sci. Pollut. Res.* **2019**, *26* (21), 21404–21415.
- (17) Ma, J. D.; Xu, J. Z.; Liu, C. H.; Yi, Q.; Zheng, M.; Cheng, L. M.; Song, T. Chemical looping combustion of sulfur paste to SO₂ by phosphogypsum oxygen carrier for sulfur acid production. *Fuel* **2022**, *323*, No. 124386.
- (18) Rosales, J.; Pérez, S. M.; Cabrera, M.; Gázquez, M. J.; Bolívar, J. P.; de Brito, J.; Agrela, F. Treated phosphogypsum as an alternative set regulator and mineral addition in cement production. *J. Cleaner Prod.* **2020**, *244*, No. 118752.
- (19) Atanasova, L. G. Exergy analysis of the process of wet-process phosphoric acid production with full utilisation of sulphur contained in the waste phosphogypsum. *Int. J. Exergy* **2010**, *7* (6), 678–692.
- (20) Xiao, J. H.; Lu, T.; Zhuang, Y. F.; Jin, H. A novel process to recover gypsum from phosphogypsum. *Materials* **2022**, *15* (5), No. 1944.
- (21) Chaalal, O.; Madhuranthakam, C. M. R.; Moussa, B.; Hossain, M. M. Sustainable approach for recovery of sulfur from phosphogypsum. *ACS Omega* **2020**, *5* (14), 8151–8157.
- (22) Xu, P. J.; Li, H.; Chen, Y. X. Experimental Study on optimization of phosphogypsum suspension decomposition conditions under double catalysis. *Materials* **2021**, *14* (5), No. 1120.
- (23) Mittal, A.; Rakshit, D. Utilization of cement rotary kiln waste heat for calcination of phosphogypsum. *Therm. Sci. Eng. Prog.* **2020**, *20*, No. 100729.
- (24) Potgieter, J. H.; Potgieter, S. S.; McCrindle, R. L.; Strydom, C. A. An investigation into the effect of various chemical and physical treatments of a South African phosphogypsum to render it suitable as a set retarder for cement. *Cem. Concr. Res.* **2003**, *33* (8), 1223–1227.
- (25) Wang, Y.; Wang, J. Z.; Zhang, Z. Y.; Yang, L.; Yan, X. S.; Zhong, B. H.; et al. Investigation of the fusion characteristics of ash in the reduction of pyrite and phosphogypsum. *J. Sustainable Metall.* **2017**, *3* (4), 737–752.
- (26) Ying, G. L.; Zhou, M. K.; Li, B. X. Experimental studies and technology process on phosphogypsum decomposition for producing sulfuric acid and lime. *Appl. Mech. Mater.* **2011**, *69*, 103–107.
- (27) Xu, Y.; Li, J. X.; Kan, L. L. Investigation on a new hydraulic cementitious binder made from phosphogypsum. *Adv. Mater. Res.* **2014**, 864–867, 1923–1928.
- (28) Lu, D. H.; Chen, Q. L.; Li, C. Q.; Gong, S. Effect of potassium feldspar on the decomposition rate of phosphogypsum. *J. Chem. Technol. Biotechnol.* **2021**, *96* (2), 374–383.
- (29) Shi, T.; Wan, T. M.; Zhang, Z. Y.; Yang, X. S.; Yang, L.; Zhong, B. H.; et al. Effect of SiO₂ on the melting characteristics of reaction between phosphogypsum and calcium sulfide. *J. Therm. Anal. Calorim.* **2016**, *123*, 1601–1609.
- (30) Zhang, H.; Chai, W. C.; Cao, Y. J. Flotation separation of quartz from gypsum using benzyl quaternary ammonium salt as collector. *Appl. Surf. Sci.* **2022**, *576*, No. 151834.
- (31) Li, X.; Lv, X. F.; Xiang, L. Review of the state of impurity occurrences and impurity removal technology in phosphogypsum. *Materials* **2023**, *16* (16), No. 5630.
- (32) Fang, J.; Ge, Y. Y.; Chen, Z. J.; Xing, B. L.; Bao, S. X.; Yong, Q.; et al. Flotation purification of waste high-silica phosphogypsum. *J. Environ. Manage.* **2022**, *320*, No. 115824.
- (33) Wang, M. S.; Yuan, X.; Dong, W. Y.; Fu, Q.; Ao, X. Q.; Chen, Q. L. Gradient removal of Si and P impurities from phosphogypsum and preparation of anhydrous calcium sulfate. *J. Environ. Chem. Eng.* **2023**, *11* (3), No. 110312.
- (34) Yang, J.; Ma, L. P.; Yang, J.; Guo, Z. Y.; Liu, H. P.; Zhang, W.; Wang, L. Gasification performance and mechanism of high-Silicon phosphogypsum oxygen carrier in Chemical Looping Gasification. *Energy Fuels* **2019**, *33* (11), 11768–11780.
- (35) Liu, C.; Zhang, Y. Z.; Li, J.; Li, J. G.; Kang, Y. Thermodynamic simulation on mineralogical composition of CaO-SiO₂-Al₂O₃-MgO quaternary slag system. *SpringerPlus* **2016**, *5* (1), No. 1028.
- (36) Du, P. P.; Zhang, Y. Z.; Long, Y.; Xing, L. Effect of the acidity coefficient on the properties of molten modified blast furnace slag and those of the produced slag fibers. *Materials* **2022**, *15* (9), No. 3113.
- (37) Chen, Z. W.; Wang, H.; Wang, M. H.; Liu, L. L.; Wang, X. D. Investigation of cooling processes of molten slags to develop multilevel control method for cleaner production in mineral wool. *J. Cleaner Prod.* **2022**, *339*, No. 130548.
- (38) Wang, W. L.; Dai, S. F.; Zhang, T. S.; Zhang, H. L.; Li, Z. M.; Xie, Y. J. The effect of CaO on the crystallization properties and viscosity of synthetic silicomanganese waste slag for mineral wool production. *J. Cleaner Prod.* **2021**, *288*, No. 125603.
- (39) Zhao, G. Z.; Zhang, L. L.; Cang, D. Q. Pilot trial of detoxification of chromium slag in cyclone furnace and production of slag wool fibres. *J. Hazard. Mater.* **2018**, *358*, 122–128.
- (40) Tian, T. L.; Jin, X. Y.; Zhang, Y. Z.; Long, Y.; Kou, X. L.; Yang, J. Y. The effect of acidity coefficient on the crystallization properties and viscosity of modified blast furnace slag for mineral wool production. *Materials* **2022**, *15* (13), No. 4606.
- (41) Zhang, T. S.; Wu, F. F.; Yang, J. Effect of basicity on the flow and crystallization behavior of synthetic nickel-iron alloy residue. *Ceram. Int.* **2023**, *49*, 17067–17073.
- (42) Ma, L. P.; Ning, P.; Zheng, S. C.; Niu, X. K.; Zhang, W.; Du, Y. L. Reaction mechanism and kinetic analysis of the decomposition of phosphogypsum via a solid-state reaction. *Ind. Eng. Chem. Res.* **2010**, *49* (8), 3597–3602.
- (43) Low, N. M. P. Observation of chemical hydration in inorganic mineral fibres. *J. Mater. Sci.* **1986**, *21* (3), 998–1004.
- (44) Nguyen, N. L.; Vu, P. L. Eco-friendly Super Sulphated Cement Concrete Using Vietnam Phosphogypsum and Sodium Carbonate Na₂CO₃. *Civ. Eng. J.* **2022**, *8* (11), 2445–2460.
- (45) Nistratov, A. V.; Klimentko, N. N.; Pustynnikov, I. V.; Vu, L. K. Thermal Regeneration and Reuse of Carbon and Glass Fibers from Waste Composites. *Emerging Sci. J.* **2022**, *6* (5), 967–984.
- (46) Zhao, S. Q.; Ma, L. P.; Yang, J.; Zheng, D. L.; Liu, H. P.; Yang, J. Mechanism of CO₂ Capture Technology Based on the Phosphogypsum Reduction Thermal Decomposition Process. *Energy Fuels* **2017**, *31* (9), 9824–9832.
- (47) Zheng, S. C.; Ning, P.; Ma, L. P.; Niu, X. K.; Zhang, W.; Chen, Y. H. Reductive decomposition of phosphogypsum with high-sulfur-concentration coal to SO₂ in an inert atmosphere. *Chem. Eng. Res. Des.* **2011**, *89* (12), 2736–2741.
- (48) Li, J.; Liu, W. X.; Zhang, Y. Z.; Yang, A. M.; Zhao, K. Research on modifying blast furnace slag as a raw material of slag fiber. *Mater. Manuf. Processes* **2015**, *30* (3), 374–380.

- (49) Jing, H. Q.; Hou, C. H.; Wang, H. B.; Yao, Y.; Liu, B. B. Slag Activation in the carbothermic reduction of Phosphorite with Adding Micronutrient-Bearing Cosolvents. *JOM* **2021**, *73* (3), 941–950.
- (50) Zhang, L.; Liu, B. B.; Zhang, Y. B.; Han, G. H.; Huang, J. J.; Ye, J.; Li, Y. New perspective on the interface reaction and morphology evolution in the reduction of manganese silicate for silicomanganese alloy production. *Appl. Surf. Sci.* **2021**, *539*, No. 148210.
- (51) Ma, D.; Wang, Q. Experimental study of CaS preparation from lignite-reduced phosphogypsum in a fluidized bed. *J. Chem. Technol. Biotechnol.* **2023**, *98* (3), 756–772.
- (52) Nengovhela, N. R.; Strydom, C. A.; Maree, J. P.; Oosthuizen, S.; Theron, D. J. Recovery of sulphur and calcium carbonate from waste gypsum. *Water SA* **2007**, *33* (5), 741–747.
- (53) Feng, H.; Xie, R. S. Phosphogypsum pyrolysis with mineralization agent under weak reducing atmosphere. *IOP Conf. Ser.: Earth Environ. Sci.* **2019**, *295* (5), No. 052030.
- (54) Msila, X.; Barnard, W.; Billing, D. G. Raman spectroscopic study of phosphogypsum thermal reduction with the carbonaceous material. *Spectrochim. Acta, Part A* **2015**, *149*, 317–322.
- (55) Mihara, N.; Kuchar, D.; Kojima, Y.; Matsuda, H. Reductive decomposition of waste gypsum with SiO_2 , Al_2O_3 , and Fe_2O_3 additives. *J. Mater. Cycles Waste Manage.* **2007**, *9*, 21–26.
- (56) Yang, J.; Zhu, B.; Ma, L. P.; Liu, H. P. Investigation of Al_2O_3 and Fe_2O_3 transmission and transformation during the decomposition of phosphogypsum. *Chin. J. Chem. Eng.* **2019**, *27* (5), 1125–1331.
- (57) van der Merwe, E. M.; Strydom, C. A.; Potgieter, J. H. Thermogravimetric analysis of the reaction between carbon and $\text{CaSO}_4 \cdot 2\text{H}_2\text{O}$, gypsum and phosphogypsum in an inert atmosphere. *Thermochim. Acta* **1999**, *340*–341, 431–437.
- (58) Ghahremaninezhad, A.; Dixon, D. G.; Asselin, E. Electrochemical and XPS analysis of chalcopyrite (CuFeS_2) dissolution in sulfuric acid solution. *Electrochim. Acta* **2013**, *87*, 97–112.
- (59) Grosvenor, A. P.; Kobe, B. A.; Biesinger, M. C.; McIntyre, N. S. Investigation of multiplet splitting of Fe2p XPS spectra and bonding in iron compounds. *Surf. Interface Anal.* **2004**, *36*, 1564–1574.
- (60) Descotes, M.; Mercier, F.; Thromat, N.; Beaucaire, C.; Gautier-Soyer, M. Use of XPS in the determination of chemical environment and oxidation state of iron and sulfur samples: constitution of a data basis in binding energies for Fe and S reference compounds and applications to the evidence of surface species of an oxidized pyrite in a carbonate medium. *Appl. Surf. Sci.* **2000**, *165* (4), 288–302.
- (61) Kumar, V.; Mishra, V.; Pitale, S. S.; Nagpure, I. M.; Coetsee, E.; Ntwaeborwa, O. M.; et al. Surface chemical reactions during electron beam irradiation of nanocrystalline $\text{CaS} : \text{Ce}^{3+}$ phosphor. *J. Appl. Phys.* **2010**, *107* (12), No. 123533.
- (62) Wang, B. W.; Li, H. Y.; Liang, Y. C.; Lv, L. L.; Mei, D. F.; Ding, N.; Zhao, H. Chemical looping combustion characteristics of coal with a Novel $\text{CaSO}_4 \cdot \text{Ca}_2\text{CuO}_3$ mixed oxygen carrier. *Energy Fuels* **2020**, *34* (6), 7316–7328.
- (63) Krylova, V.; Andrulevičius, M. Optical, XPS and XRD studies of semiconductivity copper sulfide layers in a polyamide film. *Int. J. Photoenergy* **2009**, *2009*, No. 304308.
- (64) Bahadur, S.; Gong, D.; Anderegg, J. Investigation of the influence of CaS , CaO and CaF_2 fillers on the transfer and wear of nylon by microscopy and XPS analysis. *Wear* **1996**, *197* (1), 271–279.
- (65) Fantauzzi, M.; Elsener, B.; Atzei, D.; Rigoldi, A.; Rossi, A. Exploiting XPS for the identification of sulfides and polysulfides. *RSC Adv.* **2015**, *5* (93), 75953–75963.
- (66) Liu, S.; Yang, C.; Zhang, T.; Liu, W.; Jiao, F.; Qin, W. Effective recovery of calcium and sulfur resources in FGD gypsum: Insights from the mechanism of reduction roasting and the conversion process of sulfur element. *Sep. Purif. Technol.* **2023**, *314*, No. 123537.
- (67) Bi, Y. X.; Xu, L.; Yang, M.; Chen, Q. L. Study on the effect of the activity of anthracite on the decomposition of phosphogypsum. *Ind. Eng. Chem. Res.* **2022**, *61*, 6311–6321.
- (68) Xu, Y.; Zhang, Y. Z.; Hou, L. Y.; Lu, X. Preparation of $\text{CaO} \cdot \text{Al}_2\text{O}_3 \cdot \text{SiO}_2$ system glass from molten blast furnace slag. *Int. J. Miner., Metall. Mater.* **2014**, *21*, 169–174.



CAS BIOFINDER DISCOVERY PLATFORM™

PRECISION DATA FOR FASTER DRUG DISCOVERY

CAS BioFinder helps you identify targets, biomarkers, and pathways

Unlock insights

CAS 
A division of the
American Chemical Society